High-resolution forest carbon flux mapping and monitoring in the Pacific Northwest with time since disturbance and disturbance legacies inferred from remote sensing and inventory data

Huan Gu[1], Christopher A. Williams[1], Bardan Ghimire[1,2], Feng Zhao[3], Chengquan Huang[3]

[1]Graduate School of Geography, Clark University, Worcester, MA 01610, USA
[2]Earth Sciences Division, Lawrence Berkeley National Laboratory, Berkeley, CA 94720, USA
[3]Department of Geographical Sciences, University of Maryland, College Park, MD 20742, USA

Correspondence to: Huan Gu (HuGu@clarku.edu, guhuan114031@gmail.com)

Abstract. Assessment of forest carbon storage and uptake is central to understanding the role forests play in the global carbon cycle and policy-making aimed at mitigating climate change. Current U.S. carbon stocks and fluxes are monitored and reported at fine-scale regionally, or coarse-scale nationally. We proposed a new methodology of quantifying carbon uptake and release across forested landscapes in the Pacific Northwest (PNW) at a fine scale (30 m) by combining remote-sensing based disturbance year, disturbance type, and aboveground biomass with forest inventory data in a carbon modelling framework. Time since disturbance is a key intermediate determinant that aided the assessment of disturbance-driven carbon emissions and removals legacies. When a recent disturbance was detected, time since disturbance can be directly determined by remote sensing-derived disturbance products; and if not, time since last stand-clearing was inferred from remote sensing-derived 30 m biomass map and field inventory-derived species-specific biomass regrowth curves. Net ecosystem productivity (*NEP*) was further mapped based on carbon stock and flux trajectories that described how *NEP* changes with time following harvest, fire, or bark beetle disturbances of varying severity. Uncertainties from biomass map and forest inventory data were propagated by probabilistic sampling to provide a probabilistic, statistical distribution of stand age and *NEP* for each forest pixel. We mapped mean, standard deviation and statistical distribution of stand age and *NEP* at 30 m in the PNW region. Our map indicated a net ecosystem productivity of 5.2 Tg C y^{-1} for forestlands circa 2010 in the study area, with net uptake in relatively mature (>24 year old) forests (13.6 Tg C y^{-1}) overwhelming net negative NEP from tracts that have seen recent harvest (-6.4 Tg C y^{-1}), fires (-0.5 Tg C y^{-1}), and bark beetle outbreaks (-1.4 Tg C y^{-1}). The approach will be applied to forestlands in other regions of the conterminous U.S. to advance a more comprehensive monitoring, mapping and reporting the carbon consequences of forest change across the U.S.

1 Introduction

Time since disturbance is a key determinant of ecosystem structure, composition, and function (Jenny, 1980; Chapin et al., 2012). It is a primary control on temperate forest tree height, stand biomass, demography, species composition, and vertical

structure (Hobbs and Huenneke, 1992). Considering time since disturbance is therefore essential for quantifying and predicting a wide range of ecological functions, including carbon storage and uptake (Bradford et al., 2008) which is the central focus of this paper.

A number of important prior works have sought to incorporate time since last stand-clearing disturbance (a.k.a. forest stand age) as a determinant of carbon fluxes and stocks (Cohen et al., 1996; Chen et al., 2002; Chen et al., 2003; Law et al., 2004; Turner et al., 2004; Liu et al., 2011; Pan et al., 2011; Williams et al., 2012; Zhang et al., 2012; Williams et al., 2014). High severity, stand replacing events that level all canopy dominants and even understory individuals leave a clearer mark of disturbance timing with often long-lasting legacy effects (Schoennagel et al., 2004). Forest inventories, such as Forest Inventory and Analysis (FIA), regularly attempt to characterize time since stand-replacing disturbance by recording stand age from the coring and dating of large trees in forest plots (FIA, 2015). However, for low severity events time since disturbance can be difficult to quantify in field surveys. Though this is an imperfect surrogate for time since disturbance given successional replacement of canopy dominants, it remains one of the only ways of quantifying this important attribute. Aboveground live biomass is itself a sort of record of the time since disturbance in so far as biomass exhibits a general accumulation following stand replacement. The rate of biomass accumulation is influenced by a wide range of factors such as soils and site fertility, climate setting, species composition, successional dynamics, the type of stand-replacing disturbance, and impacts from low to moderate severity disturbance events (Johnson et al., 2000). The complex combination of how these factors are distributed across landscapes challenges generic characterization of forest carbon dynamics post-replacement. However, detailed observations at local to regional scales can yield more predictable and ordered patterns as needed for large-scale mapping and monitoring (Cohen et al., 1996; Cohen et al., 2002; Harmon et al., 2004; Law et al., 2004; Turner et al., 2004; Turner et al., 2007; Turner et al., 2015).

Large area assessments of forest carbon stocks and fluxes require spatially extensive, and ideally continuous, characterization of time since disturbance across landscapes at a scale of disturbance events themselves, typically on the order of 100 m or less. Disturbance events are highly heterogeneous in space, with both occurrence and severity varying interactively with a wide range of site factors such as topography, species distributions, and legacies from past disturbances (Turner, 2010). Field inventories and surveys can characterize broad-scale disturbance rates and impacts but are rarely, if ever, extensive enough for spatially continuous characterization of disturbance events and impacts (Thomas et al., 2011). Thus, field inventory imputed carbon stocks and fluxes can only provide rough guidance for forest carbon management, monitoring and verification (Wilson et al., 2013).

A number of remote sensing techniques and associated data products are available to quantify disturbance timing, disturbance impact, and post-disturbance conditions. For example, remote sensing techniques are providing spatially extensive characterization of contemporary disturbance events and magnitude providing a direct estimate of time since disturbance (e.g. Goward et al., 2008; Huang et al., 2010; Hanson et al., 2013). Such products miss small scale events and extend only so far back in time, thus missing the long-lasting legacies from disturbances that occurred before the beginning of remote sensing observations. Long lasting legacy effects may be partially captured in RS derived estimates of

aboveground biomass and three dimensional forest structure, each estimated with optical, radar and/or lidar techniques (e.g. Kellndorfer et al., 2013; Saatchi et al., 2011). These data products have the potential to support inferences about additional properties of a given forest stand such as stand age and legacy disturbance emissions, particularly when considered within a well-defined regional context of what is typical for a local set of edaphic, climatic, and forest-type settings. There may be considerable ambiguity and confusion arising from incomplete information as well as the potential for a range of field conditions that yield similar aboveground biomass or forest structure. Nonetheless, remote sensing-derived maps of forest biomass and structure still provide a way forward to capture at least some of the information that is missing but needed for quantifying carbon stock recovery and carbon uptake and release rates over large areas.

Previous studies have mapped forest stand age at resolutions of 250 m and 1 km by generating Voronoi polygons based on FIA plot stand age data (Pan et al., 2011). Such efforts are significantly limited by sparse plot coverage, as well as the fact that stand age, disturbance legacies, and carbon stocks and fluxes all vary widely at 250 m and coarser scales but get reduced singular representations. This renders prior efforts as less appropriate for fine-scale carbon stock and flux monitoring. One aim of this paper is to address such limitations by introducing a method for inferring a stand's representative time since disturbance, relying on RS-derived biomass and disturbance products at the 30 m combined with FIA data characterizing the locally-typical rate of biomass accumulation for a given forest type group, climate, and site productivity setting. Besides, when time since disturbance was estimated from biomass data, we provided the distribution of the estimate for each pixel by propagating uncertainties from remote sensing and forest inventory derived data. The fine-scale (30 m) intermediate map of time since disturbance is then used to aid mapping of net ecosystem productivity (*NEP*) at 30 m with explicit consideration of disturbance type and severity. The larger aim is to apply the method in future work to other regions of the conterminous US in support of large scale carbon monitoring, reporting, and management.

2 Materials and Methods

2.1 Overview

Time since disturbance for each forest pixel was identified with one of the following two approaches depending on whether a recent disturbance was detected with a spectrally-based indicator of forest disturbances. For those pixels that have been mapped as having a recent disturbance, time since disturbance was directly estimated by the difference between the map year and the year of the last observed disturbance. For forest pixels that were not disturbed during the time span of the disturbance product, we inferred time since last stand-clearing disturbance, which is also called "stand age" (Masek and Collatz, 2006); terms "time since disturbance" and "stand age" are used interchangeably for undisturbed forest pixels thereafter. It was inferred from remote sensing-derived biomass data by finding the typical stand age that corresponds to each pixel's biomass according to field inventory-derived biomass-age curves, known as yield tables in forestry. The curves were sampled from FIA data and specific to forest type group and site productivity class. Consequently, maps of forest type group and site productivity aid pixel-level determination of which biomass-age curve is to be used for each pixel.

Net ecosystem productivity (*NEP*) across the PNW region was mapped based on carbon stock and flux trajectories developed in our prior work describing how *NEP* changes with time following harvest, fire, or bark beetle disturbances of varying severity. *NEP* curves with time since disturbance vary by forest type and site productivity class, and are unique to post-harvest (Williams et al. 2012), post-fire (Ghimire et al., 2012) and post-bark beetle (Ghimire et al., 2015) disturbance

5 types. *NEP* trajectories were applied to pixels with attributes of time since disturbance, forest type group, site productivity class, disturbance type, and disturbance severity to estimate carbon fluxes in forests caused by post-disturbance growth and decomposition locally and regionally.

2.2 Inferring time since disturbance from remote sensing and inventory data

2.2.1 Time since disturbance for disturbed forest pixels

10 North American Forest Dynamics (NAFD) disturbance products, Monitoring Trends in Burn Severity (MTBS) and Aerial Detection Surveys (ADS) polygons were used to determine whether and when forest pixels were disturbed during 1986 to 2010 (Fig. 1). NAFD products include 25 annual and two time-integrated forest disturbance maps with spatial resolution of 30 m for the conterminous United States (CONUS) (Goward et al., 2015). These maps were derived from annual time series Landsat images from 1986 to 2010 using the Vegetation Change Tracker (VCT) algorithm (Huang et al., 2009; Huang et al.,

15 2010). In this paper, we used one of the time-integrated data layers, which maps the year of the most recent forest disturbance between 1986 and 2010. The MTBS project maps annual burned area and burn severity at 30 m resolution across all lands of the United States from 1984 to 2014 (Eidenshink et al., 2007). Burned areas were determined by the differenced Normalized Burn Ratio (dNBR) index calculated across time-series Landsat images. MTBS defines burn severity classes based on distribution of dNBR values and ecological settings. We integrated the annual MTBS data from 1986 to 2010 into

20 two images: (1) year of the most recent fire event and (2) burn severity corresponding to the recent fire, and applied a NAFD forest area mask to the integrated maps. The ADS program conducts annual surveys to investigate forest injury caused by insect outbreaks using aircraft observations since 1997, and generates polygons recording a number of attributes including disturbance year, areas and number of trees killed by insects per area. We selected polygons attacked by bark beetles from 1997 to 2010, converted the number of trees killed by bark beetles per area to biomass killed per area by multiplying county-

25 level FIA-derived average aboveground biomass per tree for corresponding forest types, and then binned biomass killed per area into different bark beetle severity levels (Ghimire et al., 2015). Those polygons were rasterized into two images with a cell size of 30 m: (1) year of bark beetle occurrence and (2) the severity of bark beetle outbreak represented by the amount of live biomass killed, with a NAFD forest mask applied to these two images.

Preprocessed layers of NAFD (Fig. 2a), MTBS (Fig. 2b) and ADS (Fig. 2c) data characterized the year of most recent

30 disturbance events. These three layers were integrated to create a single 30 m resolution image of disturbance type associated with the last disturbance between 1986 and 2010. Since the NAFD disturbances have not yet been fully attributed to disturbance type, and because some pixels are recorded as having experienced more than one disturbance type, we made

four simplistic rules to define a single disturbance type to each pixel. These assumptions are based on the rationale that MTBS records most of the notable fire events in the region, that harvest events are one of the most ubiquitous stand replacing disturbance types active in the region, and that ADS-mapped polygons of bark beetle infestations often include unaffected stands as has been reported in the literature (Meddens et al., 2012; Vanderhoof et al., 2014). Our four rules were:

5 (1) When NAFD and MTBS overlap, if the two events are within 3 years we assigned fire to the pixel, and if the two were separated by more than 3 years, we assigned whichever event type was most recent event with harvest for NAFD, and fire for MTBS. (2) When NAFD and ADS overlap, if the two events were separated by more than 3 years, harvest was assigned to the overlapping areas, but if they occurred within three years of each other, bark beetle outbreak was assigned. (3) When MTBS and ADS overlap, the overlapping areas were assigned fire. (4) Harvest was assigned to all remaining disturbed

10 pixels identified by NAFD. The year of last disturbance for each disturbed pixel was then assigned based on the year of disturbance in each corresponding disturbance data product. The target year for mapping stand age and carbon fluxes in this paper was 2010, so time since disturbance for disturbed pixels was calculated as the difference between 2010 and the year of last disturbance.

2.2.2 Time since disturbance for undisturbed forest pixels

15 For the remaining forest pixels having no disturbance detected during 1986 to 2010, national biomass datasets were used to identify the corresponding stand age inferred from biomass-age curves that are specific to forest type groups and site productivity classes (Fig. 1). Mapped strata of forest type group and site productivity were used to determine the appropriate biomass-age curve to be used in referring stand age from biomass.

Biomass-age curves were derived from the FIA database, sampled to provide means and sampling errors for two attributes:

20 aboveground dry weight of live trees and area of forest land. The ratio of these two attributes provides aboveground live wood biomass per area. We obtained the ratios and associated errors for the PNW region through the USDA Forest Service FIA EVALIDator online tool (http://apps.fs.fed.us/Evalidator/evalidator.jsp). This yielded biomass per area within strata of forest type groups (28 classes), stand age (age class from 0-20 to 200+ years) and site productivity (7 classes). We combined the original 7 site productivity classes into high and low productivity classes, defined by the rate of forest volume growth as

25 120 to 225+ cubic feet/acre/year and 20 to 119 cubic feet/acre/year respectively. Ratios and sampling errors were recalculated for each forest type group, age class and site productivity based on this grouping. Biomass-age curves were fitted following Williams et al. (2012) by parameterizing a wood production model that best matches the field inventory data. A Monte Carlo approach was used to incorporate uncertainty in the biomass per unit area with one hundred samples of the biomass at each age class drawn probabilistically. We then fitted corresponding one hundred curves for each forest type

30 and productivity class, providing a distribution of biomass at each stand age from years 1 to 200.

Pixel-level biomass was obtained from the National Biomass and Carbon data set for the Year 2000 (NBCD 2000) (Fig. 3a). The 30 m resolution biomass map was developed based on empirical modeling combining FIA data, InSAR data from 2000 SRTM, and Landsat ETM+ optical remote sensing (Kellndorfer et al., 2012). Only biomass estimates for undisturbed pixels

were used for inferring stand age. Differences in forest masks led to a number of pixels having a biomass recorded as zero. These were replaced by the mean biomass of other undisturbed pixels with the same forest type and site productivity within this region. The 250 m forest type group maps we used were created by USDA Forest Service, and were derived from MODIS composite images in combination with FIA data and nearly 100 other geospatial data layers, portraying 28 forest

5   type groups across the contiguous United States (Ruefenacht et al., 2008) (Fig. 3b). Differences in map resolution between disturbance and forest type maps led forest type to be undefined for some pixels along forest edges, so we assigned the forest types of the nearest pixel. Site productivity maps were also derived from FIA data (Fig. 3c) with the following procedure. The FIA dataset was sampled to obtain the area of each county across the region that is of each forest type group and site productivity class. We then created a continuous map of county numbers on a 0.01 degree grid, overlayed forest types, and

10   integrated those with the data on each county's area of high and low productivity classes for the forest type that was most abundant in the pixel. This yielded a map of productivity class fractions, where each pixel has a fraction high productivity (summed over classes 1 to 3 spanning 120 to 225+ cubic feet/acre/year) and fraction low productivity (summed over classes 4 to 6 spanning 20 to 119 cubic feet/acre/year). In reality, site productivity is unlikely to vary across the 30 m pixel scale as much as it does at the county scale, whereas high and low site productivity fractions are likely to vary across counties in

15   some cases. However, an improved characterization is not available at this time.

For each undisturbed forest pixel, we extracted its biomass (B), forest type (T) and fraction of high productivity (f_{high}), and then retrieved 100 biomass trajectories for forest type T and for high and low productivity classes respectively. If the pixel was located at a high productivity site ($f_{high} = 1$), we treated 100 biomass curves for high productivity as 100 biomass realizations at stand ages from 0 to 200. All the biomass values among those realizations that lie within 20% of the pixel's

20   observed B were pooled, and corresponding stand ages were derived (Fig. 4a). We then calculated the mean, standard deviation and each of the 10th quantiles from the pooled stand ages (10th, 20th, 30th, ..., 80th, 90th quantiles of stand age) (Fig. 4b). The quantiles provided a frequency distribution of stand age for the individual pixel. Similarly, if the pixel was entirely of low site productivity ($f_{high} = 0$), we followed the above steps but using trajectories for low productivity class to derive stand age distribution for low productivity (Fig. 4c). In reality, f_{high} is almost always between 0 and 1. In order to

25   reflect high/low productivity proportion of the total, we combined the two distributions above (one for high and the other for low productivity classes) by making copies of the two distributions with 10*f_{high} copies for the high productivity and 10*(1 – f_{high}) copies for the low productivity. We calculated the mean, standard deviation and quantiles from the combined distribution of stand age (Fig. 4d). Since year 2010 was the target year for our mapping of stand age and carbon fluxes while biomass maps were generated for the year 2000, we simply added 10 years to the inferred ages to get adjusted stand ages.

30   Using the above procedure across all undisturbed forest pixels, we generated maps of the mean and stand deviation of stand age. Finally, we merged the stand age map for undisturbed forest pixels with the time since disturbance map for disturbed pixels to obtain a continuous map for all the forest pixels across the study area.

2.3 Estimating *NEP* and uncertainties across the PNW region

2.3.1 Carbon flux trajectories for harvest, fire and bark beetle

Carbon flux trajectories for post-harvest, -fire and -bark beetle outbreaks were derived from our prior work (Williams et al., 2012, Ghimire et al., 2012, Ghimire et al., 2015) involving an inventory-constrained version of the Carnegie-Ames-Stanford Approach (CASA) carbon cycle process model with inclusion of disturbance processes. The disturbance processes imposed stand-replacing harvest, fire or insect-induced partial disturbance at the final stage of the modeling after a spin-up to equilibrium carbon pools and a prior disturbance with ensuing regrowth. For a given forest type, site productivity, and prior disturbance, this forest disturbance version of the CASA model simulates net primary productivity (*NPP*) and heterotrophic respiration (*Rh*) as a function of time since disturbance, and *NEP* is then calculated as the difference of *NPP* and *Rh*. A family of curves describing carbon fluxes and stocks with time since disturbance for each combination were created to represent uncertainties in the amount of biomass killed and left on site after a disturbance, the amount of biomass left live on site post-disturbance, and the rate of biomass accumulation and mortality. Thus, we obtained 20 simulations of post-harvest *NPP, Rh* and *NEP*, 25 simulations of post-fire *NPP, Rh* and *NEP* for low, medium and high fire severities, and 1 simulation of post-bark beetle *NPP, Rh* and *NEP* for 1680 bark beetle severity levels across 0 to 200 years respectively and at each forest type group and site productivity class in the PNW region. This study emphasized use of the *NEP* curves. Fig. 5 provides examples of post-disturbance *NEP* trajectories from our prior work, showing 20 simulations of post-harvest *NEP* (Fig. 5a), the average of 25 simulations of post-fire *NEP* for three different fire severities (Fig. 5b), and 1 simulation of post-bark beetle *NEP* for three examples of bark beetle disturbances that kill low, medium and high amounts of biomass (Fig. 5c) in high site productivity Douglas-fir stands in the PNW region. The typical pattern of *NEP* following a disturbance involves a large negative value immediately after disturbance, a rise for a number of years to reach a maximum rate of carbon uptake, and then a gradual decline. The full range of post-disturbance *NEP* curves across forest types, productivity classes, and disturbance types is presented in the supplementary figures (Fig. S1, S2).

2.3.2 Mapping *NEP* and uncertainties across the PNW region

The characteristic trajectories serve as look-up tables relating carbon fluxes and stocks (here just *NEP*) to years since disturbance within the strata of forest type group, site productivity fraction, disturbance type and severity. For disturbed pixels, the distribution of *NEP* corresponding to the pixel's time since disturbance and forest type was sampled for both high and low productivity classes, and then weighted according to the pixel's fraction of high site productivity (f_{high}). Weighting involved a simple repetition of each data population based on the pixel's fraction of high productivity, with $10*f_{high}$ copies for the high productivity estimates and $10*(1 - f_{high})$ copies for the low productivity population. These two populations were then combined to create a single composite distribution representing the full probability distribution for the pixel's *NEP*. A similar procedure was performed for all remaining undisturbed forest pixels but including the additional uncertainty on the pixel's stand age. We propagated stand age uncertainty by obtaining the *NEP* distribution for each of the 10*th* quantiles of

the age distribution corresponding to the pixel's biomass and forest type for both high and low productivity classes, and compositing these into a full probability distribution of the pixel's *NEP* based on the pixel's fraction of high probability (f_{high}). Finally, we calculated the mean, standard deviation and quantiles (10*th*, 20*th*, 30*th*, ..., 80*th*, 90*th* quantiles) of *NEP* distribution for each forest pixel across the PNW region.

3 Results

3.1 Disturbance maps derived from NAFD, MTBS and ADS

Across the $2.1*10^7$ ha of forest in the PNW region, harvest was recorded as having affected the largest area ($5.4*10^6$ ha from 1986-2010) followed by bark beetles ($1.8*10^6$ ha from 1997 - 2010) and then fire ($9.3*10^5$ ha from 1986 - 2010). Their distributions are displayed in Fig. 6. Reported as percentages, harvest, bark beetles, and fire affected 26%, 9%, and 5% of all forestland in the PNW during their respective time intervals. Table 1 provides an additional report of each area by forest type and for high and low productivity class sites. Douglas-fir comprises nearly 50% of all forest in the PNW, with about 70% of it being in high productivity class lands. Ponderosa Pine, Fir-Spruce-Mountain Hemlock, and Hemlock-Sitka Spruce are the next most abundant forest type groups, comprising 17%, 15%, and 7% of the PNW forest, with 16%, 39%, and 85% in high productivity sites, respectively.

About half (52%) of all harvesting occurred in Douglas-fir forests, with 20% in Ponderosa Pine stands and 8% and 7% in Fir-Spruce-Mountain Hemlock, and Hemlock-Sitka Spruce stands. Of all forestland that burned, 37% was in Douglas-fir stands, 27% in Ponderosa Pine, and 21% in Fir-Spruce-Mountain Hemlock. Hemlock-Sitka Spruce was not vulnerable to fire. Though fire affected a larger area of low productivity sites for Ponderosa Pine and Fir-Spruce-Mountain Hemlock forest types, fire occurrence was equally likely across low and high productivity classes. In contrast, Douglas-fir stands had similar burned areas for low and high productivity sites, but low productivity sites were three times as likely to experience fire. Bark beetle outbreaks were most common in Douglas-fir stands, with 40% of all outbreak area, while 30% and 18% occurred in Fir-Spruce-Mountain Hemlock and Ponderosa Pine stands, respectively. As with fire, though a larger proportion of the total bark beetle outbreak area occurred in low productivity Ponderosa Pine and Fir-Spruce-Mountain Hemlock stands, their occurrence was equally likely across low and high productivity sites. Again in contrast, Douglas-fir was seen a more even distribution of bark beetle outbreak area across productivity classes, but beetle outbreak occurrence was about three times more likely in low productivity sites. Of all Douglas-fir stands, 28% were disturbed by harvest, 3% by fire, and 7% by bark beetles. Percentages for Ponderosa Pine stands were 31%, 7%, and 9% for harvest, fire, and bark beetles, and for Fir-Spruce-Mountain Hemlock they were 13%, 6%, and 17%, Hemlock-Sitka Spruce was mainly disturbed by harvesting (28%), with 0% for fire and 5% for bark beetles.

3.2 Biomass-age curves by forest types and site productivity classes

The fitted biomass regrowth curves exhibit considerable variations across forest types and site productivity classes (Fig. 7 for Douglas-fir, Ponderosa Pine and Fir-Spruce-Mountain Hemlock). Compared to Douglas-fir forests, Ponderosa Pine forests hold only about 28% to 33% as much biomass, and Fir-Spruce-Mountain Hemlock holds about 59% to 64% as much.

5   Biomass accumulates more rapidly and to a higher maximum stock for high productivity sites for all forest types according to FIA data and corresponding model fits, achieving about 1.4 to 1.8 times the biomass at low productivity sites. But the biomass-age curves share some common features among different forest types and site productivity classes. Biomass accumulates rapidly at the early ages (~ 0-50 years), slowing down with age until it saturates often around 150-200 years. Besides, variation in biomass increases as a function of stand age both in the FIA data and in the model fits. The fitted

10   curves provided a range and distribution of biomass at each stand age from 0 to 200. Because of the simple stand-level growth equation that was assumed, these curves yielded a smoothed fit to the inventory data rather than showing a saw-toothed increase with stand age.

3.3 Maps of time since disturbance and uncertainties across the PNW region

The forested landscape is a complicated mosaic of time since last disturbance (Fig. 8a). Overall, a wide range of years are

15   spanned with abrupt discontinuities related to recent stand replacing disturbances, transitions between forest types, and transitions between site productivity classes. One feature that stands out prominently is the prevalence of recent disturbances along the eastern, drier side of the Cascade Range, resulting from both harvesting and bark beetle outbreaks (Fig. 6b). Large fires produce sizable patches with the same time since disturbance. The imprint of segments of relatively old, high-elevation forests is also evident. It should be noted that this map was not used directly in the computation of *NEP* for undisturbed

20   forest pixels, which relied instead on stand age distributions for high and low site productivity classes, but it is presented here to provide a best estimate of disturbance timing at the pixel scale.

Uncertainty on the time since disturbance for disturbed forest pixels is not currently available from disturbance products and thus was not mapped. For undisturbed forest pixels, the uncertainty of stand age was represented by standard deviation of the full stand age distribution combined from high and low site productivity and reflecting high/low productivity proportion.

25   The uncertainty map identifies locations where stand age is more tightly constrained by the data and method (Fig. 8b). Across all the stand ages inferred from the biomass data (undisturbed forest pixels), the spatially-averaged mean standard deviation of stand age is around 25 years.

3.4 Maps of NEP and uncertainties across the PNW region in Year 2010

Spatial variations in mean annual *NEP* are noticeably correlated with the time since disturbance, forest type group, and site

30   productivity strata used in the mapping procedure (Fig. 9a). There is a general pattern of weaker carbon sinks in the eastern, drier portion of the study area. Both sink strength and carbon source strength tend to be largest in the western areas of higher

biomass. Recent (< 20 years) fire and harvest disturbances tend to create focused carbon sources on the landscape, giving way to sinks as regrowth ensues. For example, one can see a clear imprint of the well-known 2002 Biscuit fire in southwestern Oregon. Area with very recent, but low severity bark beetle outbreaks have an only muted reduction in *NEP* compared to nearby undisturbed forest, remaining carbon sinks despite the disturbance episode.

5 At the regional scale, *NEP* is estimated to be 5.2 Tg C y^{-1}, or about 25.4 g C m^{-2} y^{-1} averaged for the 2.1*10^7 ha forest (Table 2). Forestlands free of recent disturbance are the region's main terrestrial carbon sink with *NEP* of 13.6 ± 3.7 Tg C y^{-1}. In contrast, *NEP* for forests disturbed by harvest, fire and bark beetles within the prior two and a half decades are estimated to be -6.4 ± 2.3 Tg C y^{-1}, -0.5 ± 0.2 Tg C y^{-1}, and -1.5 ± 0.0 Tg C y^{-1} respectively, serving as significant carbon sources. Table 2 also reports mean *NEP* by forest type groups for all forestland, and also separately for undisturbed and disturbed forests. Fir-

10 Spruce-Mountain Hemlock followed by Hemlock-Sitka Spruce and Douglas-fir were the largest carbon sinks of 1.5 Tg C y^{-1}, 1.5 Tg C y^{-1}, and 1.0 Tg C y^{-1} respectively. Considering only undisturbed forestlands, Douglas-fir was the largest carbon sink of 7.9 ± 2.1 Tg C y^{-1}, but this was mostly offset by it having also the region's largest carbon sources from harvest, fire events and bark beetle outbreaks with *NEP* of -5.7 ± 1.6 Tg C y^{-1}, -0.4 ± 0.1 Tg C y^{-1}, and -0.7 ± 0.0 Tg C y^{-1} respectively. Douglas-fir's relatively large area-integrated carbon fluxes result not only from it being the most abundant forest type in the

15 PNW region, but also its large disturbed areas and large carbon stock potential. Recently disturbed forests tend to aggregate to carbon sources. In some forest type groups we found a net carbon sink even for recently disturbed forests. For example, Lodgepole Pine had net carbon sinks for harvested and burned stands. This results from a large proportion of disturbance events having occurred early in the disturbance record allowing recovery and regrowth to overwhelm the carbon sources from the most recent events.

20 **4 Discussion**

Our method of estimating time since disturbance from disturbance products (disturbed forest pixels) or inferring stand age from biomass (undisturbed forest pixels) to estimate carbon flux and biomass accumulation relies on a number of data products and assumptions that need to be critically evaluated. First, the method assumes that field inventory data provide a reliable and well-constrained estimation of forest biomass as a function of stand age for regionally-specific strata of forest

25 type and site productivity class.

Second, the approach described here assumes that stand-level biomass is a useful predictor of stand age, biomass accumulation and net carbon flux regardless of how that stand-level biomass was approached (Zhang et al., 2014). However, a particular stand-level biomass may be reached from steady accumulation during a relatively disturbance-free interval of time, or also from a recent disturbance that reduced biomass to the current level. Information is also lacking on how the

30 biomass-age relationship varies depending on the type of stand-replacing disturbance. Such path dependency can have important implications for the true stand age as well as for post-disturbance carbon fluxes and stocks by influencing species composition, stand structure, site fertility, and other relevant factors.

Next, the carbon cycle model used to estimate carbon fluxes as a function of time since disturbance relies on a simple growth rate equation to characterize biomass accumulation over time with a constant wood turnover time regardless of stand age and a constant rate of carbon allocation to wood. It also assumes that mean annual net primary productivity is constant after an initial rise through stand initiation. These assumptions arise from limited data to describe these dynamics for the range of

5 settings active at a continental-scale but improvement may be possible with detailed explorations into regional parameterizations. Our prior work indicated some sensitivity of carbon flux estimation to these assumptions, though the impact on continental-scale carbon flux estimation was modest (Williams et al., 2012).

Lastly, the method relies on maps of aboveground biomass, forest type group, site productivity class and forest disturbance which are sure to have errors. In the biomass dataset, correlation coefficients between observed and predicted biomass were

10 estimated to be 0.62-0.75 in the PNW region (Kellndorfer et al., 2012). The accuracy of forest type group map in this region ranges from 61% to 69% (Ruefenacht et al., 2008). The ADS dataset is limited to the areas flown in the survey years, and may underestimate the number of trees killed by bark beetles but overestimate the area of affected stands (Meddens et al., 2012). Incorporation of local high-resolution high-accuracy maps for these strata into national maps can significantly reduce uncertainties in our mapping and interpretation of stand age, carbon accumulation and fluxes at fine scales (Huang et al.,

15 2015).

Our analyses have sought to incorporate three main sources of uncertainties in input data layers to estimate mean annual *NEP* for a given pixel. The first is uncertainty in the biomass defined at a pixel scale. The second source of uncertainty comes from a range of potential stand ages that could correspond to a given biomass stock. The third source of uncertainty comes from the *NEP* that we estimate for a given stand age, forest type, site productivity, and prior disturbance type and

20 severity. The first and second uncertainties were propagated to provide a probabilistic, statistical estimation of stand age. The full range distribution of stand age and the third uncertainty were further propagated by probabilistic sampling to obtain an *NEP* distribution for each forest pixel. Though pixel-level accuracies are correspondingly low for many situations, aggregation to larger scales involves spatial cancellation such that regional and continental uncertainties are much reduced relative to what would be inferred directly from the pixel scale.

25 Previous studies have used FIA and remote sensing data to map forest stand age at resolutions of 250 m and 1 km (Pan et al., 2011). In undisturbed areas, spatial pattern and density distribution of stand age between the two studies are mostly consistent (Fig. 10a, 10b), but this study has a much higher density at the age class of 0-10 years and a bit lower density at 50-100 years (Fig. 10c). There are a number of likely explanations for these discrepancies. The first is definitional, in this study we estimated time since disturbance including both partial and stand-replacing disturbances, resulting in assigning a

30 young age to an old-growth forest stand undergoing a light-severity partial disturbance; while Pan et al. (2011) mapped stand age with consideration of only stand-clearing disturbance. The second cause could be related to the years included in each study, with a large percent of forestlands disturbed by harvest, fire or bark beetles between 2000 (mapping year in Pan's study) and 2010 (mapping year in this study) (Fig. 6). Other factors that may contribute to this discrepancy include different datasets and methodology used for analysis and mapping, and different spatial resolutions between the maps. For example,

when mapping at a much coarser resolution (250 m or 1 km), fragmented disturbed forest patches are likely lost due to disturbed areas taking up a small fraction in the coarse-scale pixel, yielding stand age for those areas represented by nearby undisturbed forest stands that are more abundant in that pixel. The map of time since disturbance from this study having a spatial resolution of 30 m is able to distinguish finer differences in the stand age structure for persistent forests, but also able

5 to capture abrupt discontinuities related to recent stand replacing disturbances, transitions between forest types, and transitions between site productivity class abundances. This fine spatial detail of the data indicates the information that is lost when stand age is spatially averaged to coarser grids. Such spatial averaging of stand age becomes even more problematic when combined with the nonlinear relationships between forest properties and age, such as with biomass and *NEP*. Maps of time since disturbance and uncertainties from this study may be valuable in and of itself for various ecological

10 applications even if our purpose was generate it as an intermediate variable needed en route to accurate description of, and interpretation of, carbon stocks and fluxes.

An additional comparison was made between the distribution of forest area with age class from this study and that sampled from the FIA dataset (Fig. 11 for Douglas-fir and Fir-Spruce-Mountain Hemlock). We provided two age distributions from this study, one sampled from only undisturbed pixels and another including all forested pixels. Overall, the FIA-derived age

15 distribution agrees well with that for our undisturbed forest pixels. This is true except for in the youngest age classes when we include the pixels marked as disturbed in this study, finding a much larger frequency of young-aged forests. As noted for the comparison described above, here too we note a definition bias where we included partial, low severity disturbances as stand of young ages but which are more appropriately described as being of older stand age from 20-40 years up to 200+ years in FIA dataset. We note that this definitional issue does bias estimates of *NEP* or biomass, which are derived based on

20 severity-specific carbon stock and flux trajectories.

The PNW-wide forest *NEP* reported here (5 Tg C y^{-1}) is lower than in our earlier work (11 Tg C y^{-1}) that used similar methods (see RS-based results in Williams et al. 2014). A portion of this difference can be attributed to smaller net carbon losses from forestlands that had recent (1986 to 2010) disturbance by either harvest or fire, reported as contributing -4 Tg C y^{-1} in our earlier work but -7 Tg C y^{-1} here. Here we also include additional net carbon losses from bark beetle outbreaks (-

25 1.4 Tg C y^{-1}) that were not considered in our earlier work. The remaining discrepancy (-1.6 Tg C y^{-1}) is necessarily due to other methodological and data source innovations introduced here including (a) use of the newly available Landsat-derived forest disturbance data product that now offers full spatial coverage compared to only about 50% coverage previously, and (b) new use of biomass data to characterize stand age and associated carbon flux patterns.

The net carbon release from recent bark beetle outbreaks (-1.4 Tg C y^{-1} in 2010) is comparable to that reported in our earlier

30 work (Ghimire et al. 2015). In our earlier work we reported that the PNW region experienced about 26% of the total beetle-killed biomass mortality in western US regions. Applying that percentage to the US west-wide *NEP* reduction of 6 to 9 Tg C y^{-1} in the year 2009 (Ghimire et al. 2015) indicates a *NEP* reduction for just the PNW of about 1.6 to 2.3 Tg C y^{-1}, just higher than the net carbon release induced by bark beetles reported here.

Additional points of comparison come from a variety of papers focused on regions of Oregon by Turner et al. (2004, 2007 & 2015). These studies report similar west versus east patterns of *NEP* across the mountain ranges of the region, and similar variation in *NEP* across forest types. However, the work of Turner et al. (2004, 2007 & 2015) tends to estimate higher *NEP* in young regenerating forests (e.g. 14 to 99 years since stand clearing) in the Coast Range and West Cascades, reaching 250

5   to 390 g C m^{-2} y^{-1} whereas our curves peak at around 245 g C m^{-2} y^{-1} for the full PNW region (Fig. S1). This discrepancy could be due to the greater spatial detail on climate patterns included in their modelling work, and also plant productivity, allocation, and turnover rates prescribed at the ecoregion-scale in the work of Turner et al. (2004, 2007 & 2015). Given our work's aim of estimating forest carbon stocks and fluxes across the full conterminous US, it is not currently feasible to assemble the data needed to perform such fine-scale ecoregional calibration even while appreciating its value.

10   **5 Conclusions**

In this paper, we introduced a new methodology for comprehensively combining remote-sensing based, 30 m resolution data on disturbance year, disturbance type, and aboveground biomass with forest inventory data in a carbon modeling framework to quantify carbon uptake and release across forested landscapes at a fine scale (30 m). Time since disturbance was an important intermediate variable that aided the assessment of disturbance-driven carbon emissions and removals legacies. We

15   mapped mean, standard deviation and statistical distribution of stand age and *NEP* that were propagated from uncertainties of input data layers by probabilistic sampling. This method was applied to the Pacific Northwest (PNW) region of the United States. Region-wide we found a net ecosystem productivity of 5.2 Tg C y^{-1} for forestlands circa 2010, with net uptake in relatively mature (>24 year old) forests (13.6 Tg C y^{-1}) overwhelming net negative *NEP* from tracts that have seen recent harvest (-6.4 Tg C y^{-1}), fires (-0.5 Tg C y^{-1}), and bark beetle outbreaks (-1.4 Tg C y^{-1}). Our proposed approach will be further

20   applied to forestlands in other regions of the conterminous US to advance a more comprehensive monitoring, mapping and reporting the carbon consequences of forest change across the US.

Acknowledgements

This study was financially supported by NASA's Carbon Monitoring System program (NNH14ZDA001N-CMS) under award NNX14AR39G.

25   **References**

Bradford, J.B., Birdsey, R.A., Joyce L.A., and Ryan M.G.: Tree age, disturbance history, and carbon stocks and fluxes in subalpine Rocky Mountain forests, Glob. Change Biol., 14, 2882–2897, 2008.

Chapin, III F.S., Matson, P.A., and Mooney, H.A.: Principles of Terrestrial Ecosystem Ecology, 2nd ed. Springer, New York, 2012.

Chen, J.M., Ju, W., Cihlar, J., Price, D., Liu, J., Chen, W., Pan, J., Black, A., and Barr, A.: Spatial distribution of carbon sources and sinks in Canada's forests based on remote sensing, Tellus, 55B: 622-641, 2003.

Chen, W., Chen, J.M., Price, D.T., and Cihlar, J.: Effects of stand age on net primary productivity of boreal black spruce forests in Canada, Canadian Journal for Forest Research, 32(5): 833-842, 2002.

Cohen, W.B., Harmon, M.E., Wallin, D.O., and Fiorella, M.: Two decades of carbon flux from forests of the Pacific Northwest, BioScience, 46, 836-844, 1996.

Cohen, W.B., Spies, T.A., Alig, R.J., Oetter, D.R., Maiersperger, T.K., and Fiorella, M.: Characterizing 23 years (1972–95) of stand replacement disturbance in western Oregon forests with Landsat imagery, Ecosystems, 5, 122–137, doi:10.1007/s10021-001-0060-X, 2002.

Eidenshink, J., Schwind, B., Brewer, K., Zhu, Z., Quayle, B., and Howard, S.: A project for monitoring trends in burn severity, Fire Ecology, 3(1), 3-21, 2007.

Forest Inventory & Analysis (FIA): USDA Forest Service National Core Field Guide Version 7.0. Available at: http://www.fia.fs.fed.us/library/field-guides-methods-proc/docs/2015/Core-FIA-FG-7.pdf, 2015.

Ghimire, B., Williams, C.A., Collatz, G.J., and Vanderhoof, M.: Fire-induced carbon emissions and regrowth uptake in western US forests: documenting variation across forest types, fire severity, and climate regions, J. Geophys. Res.-Biogeo., 117, doi:10.1029/2011JG001935, 2012.

Ghimire, B., Williams, C.A., Collatz, G.J., Vanderhoof, M., Rogan, J., Kulakowski, D., and Masek, J.G.: Large carbon release legacy from bark beetle outbreaks across Western United States, Glob. Change Biol., 21(8), 3087-3101, doi: 10.1111/gcb.12933, 2015.

Goward, S.N., Masek, J.G., Cohen, W.B., Moisen, G., Collatz, G.J., Healey, S., Houghton, R.A., Huang, C., Kennedy, R.E., Law, B.E., Powell, S., Turner, D.P., and Wulder, M.A.: Forest disturbance and North American carbon flux, EOS Transactions, American Geophysical Union, 89, 105-106, 2008.

Goward, S.N., Huang, C., Zhao, F., Schleeweis, K., Rishmawi, K., Lindsey, M., Dungan, J.L., and Michaelis, A.: NACP NAFD Project: Forest Disturbance History from Landsat, 1986-2010. ORNL DAAC, Oak Ridge, Tennessee, USA. http://dx.doi.org/10.3334/ORNLDAAC/1290, 2015.

Hansen, M.C., Potapov, P.V., Moore, R., Hancher, M., Turubanova, S.A., Tyukavina, A., Thau, D., Stehman, S.V., Goetz, S.J., Loveland, T.R., Kommareddy, A., Egorov, A., Chini, L., Justice, C.O., and Townshend, J.R.G.: High-resolution global maps of 21st-century forest cover change, Science, 342, 850-853, 2013.

Harmon, M.E., Bible, K., Ryan, M.G., Shaw, D.C., Chen, H., Klopatek, J., and Li, X.: Production, respiration, and overall carbon balance in an old-growth Pseudotsuga-Tsuga forest ecosystem, Ecosystems, 7, 498–512, 2004.

Hobbs, R.J. and Huenneke, L.F.: Disturbance, Diversity, and Invasion: Implications for Conservation, Conserv. Biol., 6(3), 324-337, 1992.

Huang, C., Goward, S.N., Masek, J.G., Gao, F., Vermote, E.F., Thomas, N., Schleeweis, K., Kennedy, R.E., Zhu, Z., Eidenshink, J.C., and Townshend, J.R.G.: Development of time series stacks of Landsat images for reconstructing forest disturbance history, International Journal of Digital Earth, 2(3), 195-218, 2009.

Huang, C., Goward, S.N., Masek, J.G., Thomas, N., Zhu, Z., and Vogelmann, J.E.: An automated approach for reconstructing recent forest disturbance history using dense Landsat time series stacks, Remote Sens. Environ., 114(1), 183-198, 2010.

Huang, W., Swatantran, A., Johnson, K., Duncanson, L., Tang, H., O'Neil-Dunne, J., Hurtt, G., and Dubayah, R.: Local discrepancies in continental scale biomass maps: a case study over forested and non-forested landscapes in Maryland, USA, Carbon Balance and Management, 10:19, doi: 10.1186/s13021-015-0030-9, 2015.

Jenny, H.: The Soil Resources: Origin and Behavior, Springer-Verlag, New York, 1980.

Johnson, C.M., Zarin, D.J., and Johnson, A.H.: Post-disturbance aboveground biomass accumulation in global secondary forests, Ecology, 81(5), 1395-1401, 2000.

Kellndorfer, J., Walker, W., Kirsch, K., Fiske, G., Bishop, J., LaPoint, L., Hoppus, M., and Westfall, J.: NACP Aboveground Biomass and Carbon Baseline Data, V. 2 (NBCD 2000), U.S.A., 2000. Dataset Available on-line [http://daac.ornl.gov] from ORNL DAAC, Oak Ridge, Tennessee, U.S.A. http://dx.doi.org/10.3334/ORNLDAAC/1161, 2013.

Law, B.E., Turner, D., Campbell, J.L., Sun, O.J., Van Tuyl, S., Ritts, W.D., and Cohen, W.B.: Disturbance and climate effects on carbon stocks and fluxes across Western Oregon USA, Glob. Change Biol., 10, 1429–1444, doi:10.1111/j.1365-2486.2004.00822.x, 2004.

Liu, S., Bond-Lamberty, B., Hicke, J.A., Vargas, R., Zhao, S., Chen, J., Edburg, S.L., Hu, Y., Liu, J., McGuire, A.D., Xiao, J., Keane, R., Yuan, W., Tang, J., Luo, Y., Potter, C., and Oeding, J.: Simulating the impacts of disturbances on forest carbon cycling in North America: Processes, data, models, and challenges, J. Geophys. Res.-Biogeo., 116, G00K08, doi:10.1029/2010JG001585, 2011.

Masek, J.G. and Collatz, G.J.: Estimating forest carbon fluxes in a disturbed southeastern landscape: Integration of remote sensing, forest inventory, and biogeochemical modelling, J. Geophys. Res.-Biogeo., 111, G01006, doi:10.1029/2005JG000062, 2006.

Meddens, A.J.H., Hicke, J.A., and Ferguson, C.A.: Spatial and temporal patterns of observed bark beetle-caused tree mortality in British Columbia and western US, Ecol. Appl., 22, 1876–1891, 2012.

Pan, Y., Chen, J.M., Birdsey, R.A., McCullough, K., He, L., and Deng, F.: Age Structure and Disturbance Legacy of North American Forests, Biogeosciences, 8, 715-732, 2011.

Ruefenacht, B., Finco, M.V., Nelson, M.D., Czaplewski, R., Helmer, E.H., Blackard, J. A., Holden, G.R., Lister, A.J., Salajanu, D., Weyermann, D., and Winterberger, K.: Conterminous U.S. and Alaska Forest Type Mapping Using Forest Inventory and Analysis Data. Photogramm, Eng. Rem. S., 74(11), 1379-1388, 2008.

Saatchi, S., Harris, N.L., Brown, S., Lefsky, M., Mitchard, E.T.A., Salas, W., Zutta, B.R., Buermann, W., Lewis, S.L., Hagen, S., Petrova, S., White, L., Silman, M., and Morel, A.: Benchmark map of forest carbon stocks in tropical regions across three continents, P. Natl. Acad. Sci. USA, 108, 9899-9904, 2011.

Schoennagel, T., Veblen, T.T., and Romme, W.H.: The interaction of fire, fuels, and climate across Rocky Mountain forests, BioScience, 54(7), 661-676, 2004.

Thomas, N.E., Huang, C., Goward, S.N., Powell, S., Rishmawi, K., Schleeweis, K., and Hinds, A.: Validation of North American Forest Disturbance dynamics derived from Landsat time series stacks, Remote Sens. Environ., 115, 19–32, 2011.

Turner, D.P., Guzy, M., Lefsky, M.A., Ritts, W.D., Van Tuyl, S., and Law, B.E.: Monitoring forest carbon sequestration with remote sensing and carbon cycle modeling, Environ. Manage., 4, 457-466, 2004.

Turner, D.P., Ritts, W.D., Law, B.E., Cohen, W.B., Yang, Z., Hudiburg, T., Campbell, J.L., and Duane, M.: Scaling net ecosystem production an net biome production over a heterogeneous region in the western United States, Biogeosciences, 4, 597-612, doi:10.5194/bg-4-597-2007, 2007.

Turner, D.P., Ritts, W.D., Kennedy, R.E., Gray, A.N., and Yang, Z .: Effects of harvest, fire, and pest/pathogen disturbances on the West Cascades ecoregion carbon balance, Carbon Balance and Management, 10:12, doi: 10.1186/s13021-015-0022-9, 2015.

Turner, M.G.: Disturbance and landscape dynamics in a changing world, Ecology, 91(10), 2833-2849, 2010.

Vanderhoof, M., Williams, C.A., Shuai, Y., Jarvis, D., Kulakowski, D., and Masek, J.G.: Albedo-induced radiative forcing from mountain pine beetle outbreaks in forests, south-central Rocky Mountains: magnitude, persistence, and relation to outbreak severity, Biogeosciences, 11, 563-575, doi:10.5194/bg-11-563-2014, 2015.

Williams, C.A., Collatz, G.J., Masek, J., and Goward, S.N.: Carbon consequences of forest disturbance and recovery across the conterminous United States, Global Biogeochem. Cy., 26, doi:10.1029/2010GB003947, 2012.

Williams, C.A., Collatz, G.J., Masek, J., Huang, C., and Goward, S.N.: Impacts of disturbance history on forest carbon stocks and fluxes: merging satellite disturbance mapping with forest inventory data in a carbon cycle model framework, Remote Sens. Environ., 151, 57–71, 2014.

Wilson, B.T., Woodall, C.W., and Griffith, D.M.: Imputing forest carbon stock estimates from inventory plots to a nationally continuous coverage, Carbon Balance and Management, 8:1, doi: 10.1186/1750-0680-8-1, 2013.

Zhang, F., Chen, J.M., Pan, Y., Birdsey, R.A., Shen, S., Ju, W., and He, L.: Attributing carbon changes in conterminous US forests to disturbance and non-disturbance factors from 1901 to 2010, J. Geophys. Res.-Biogeo., 117, G02021, doi:10.1029/2011JG001930, 2012.

Zhang, C., Ju, W., Chen, J.M., Li, D., Wang, X., Fan, W., Li, M., and Zan, M.: Mapping forest stand age in China using remotely sensed forest height and observation data, J. Geophys. Res.-Biogeo., 119, 1163-1179, doi: 10.1002/2013JG002515, 2014.

Table 1. Area (ha) of all forest lands, forests disturbed by harvest (1986-2010), fire (1986-2010) and bark beetle (1997-2010) by forest type groups, and for high and low site productivity classes in the PNW region.

Forest Type Group*	All Forest		Harvested		Burned		Bark Beetle Infested	
	High	Low	High	Low	High	Low	High	Low
Douglas-fir	6909151	3097083	2039661	752902	161221	181147	301234	416181
Ponderosa Pine	565633	2953701	188300	888668	39135	213925	53982	261530
Fir/Spruce/Mountain Hemlock	1220916	1914562	155898	250135	61140	135947	193838	343326
Hemlock/Sitka Spruce	1168836	211376	338263	45762	255	226	54352	19382
Pinyon/Juniper	79800	664050	10561	84517	2988	27601	250	1378
Alder/Maple	633369	43005	278797	18128	325	24	3442	290
Lodgepole Pine	135874	441717	38737	167320	13064	42235	22692	78753
Western Oak	52774	97472	15572	25392	4371	7817	1036	2026
California Mixed Conifer	16841	73817	5017	18369	550	1669	836	1376
Tanoak/Laurel	50897	26536	11291	5351	6431	3509	265	160
Other Western Hardwoods	39696	33718	10542	7342	535	844	912	777
Elm/Ash/Cottonwood	34093	17945	14779	7812	331	284	60	41
Western Larch	20464	28342	3126	4611	744	1436	5078	6597
Other Western Softwood	9956	24206	1441	2587	1711	6037	1726	5259
Western White Pine	7877	4471	204	183	7360	3951	35	37
Aspen/Birch	1908	2607	730	894	176	286	124	353

*Forest type groups are ordered by the forest areas from largest to smallest.

1   **Table 2.** Mean net ecosystem productivity (*NEP*) and total net carbon uptake by forest type group in all forest, undisturbed forest, forests
2   disturbed by harvest, fire and bark beetle occurred during time spam of remote sensing disturbance products.

Forest Type Group*	All Forest		Undisturbed Forest		Harvested		Burned		Bark Beetle Infested	
	Mean NEP	Total NEP	Mean NEP	Total NEP	Mean NEP	Total NEP	Mean NEP	Total NEP	Mean NEP	Total NEP
	(g C m^{-2} y^{-1})	(Gg C y^{-1})	(g C m^{-2} y^{-1})	(Gg C y^{-1})	(g C m^{-2} y^{-1})	(Gg C y^{-1})	(g C m^{-2} y^{-1})	(Gg C y^{-1})	(g C m^{-2} y^{-1})	(Gg C y^{-1})
Douglas-fir	10.4	1036.3	128.6	7912.6	-205.7	-5745.7	-130.0	-445.0	-96.3	-687.9
Ponderosa Pine	15.8	557.7	47.4	887.9	-14.8	-159.2	-3.0	-7.7	-52.0	-163.6
Fir/Spruce/Mountain Hemlock	48.8	1529.4	108.3	2161.6	-22.0	-89.5	-35.0	-69.0	-88.6	-475.0
Hemlock/Sitka Spruce	107.0	1477.0	197.0	1816.6	-76.7	-294.6	-106.3	-0.5	-61.0	-44.9
Pinyon/Juniper	5.2	38.9	9.4	58.2	-18.7	-17.8	-1.9	-0.6	-57.5	-0.9
Alder/Maple	58.4	395.3	118.0	442.8	-16.7	-49.7	97.6	0.3		
Lodgepole Pine	6.6	38.1	36.6	78.6	4.2	8.6	28.2	15.6	-63.8	-64.7
Western Oak	9.5	14.2	28.4	26.7	-33.9	-13.9	5.8	0.7		
California Mixed Conifer	14.2	12.9	27.0	17.0	-19.5	-4.6	70.3	1.6	-61.5	-1.1
Tanoak/Laurel	79.0	61.2	161.8	81.6	-82.3	-13.7	-73.4	-7.3		
Other Western Hardwoods	43.7	32.1	62.0	32.5	-12.4	-2.2	59.5	0.8		
Elm/Ash/Cottonwood	29.9	15.6	119.4	34.3	-81.6	-18.4	-61.6	-0.4		
Western Larch	33.8	16.5	97.2	26.5	-34.7	-2.7	-21.1	-0.5	-58.6	-6.8
Other Western Softwood	-14.3	-4.9	26.4	4.1	-21.8	-0.9	-39.9	-3.1	-71.6	-5.0
Western White Pine	35.8	4.4	4.8	0.0	-14.6	-0.1	39.8	4.5	-69.0	0.0
Aspen/Birch	20.3	0.9	51.6	1.0	-14.8	-0.2	-9.8	0.0		
Total	25.4	5225.5	108.8	13581.8	-118.8	-6404.5	-55.1	-510.5	-82.3	-1438.1

3   *Forest type groups are ordered by the forest areas from largest to smallest.
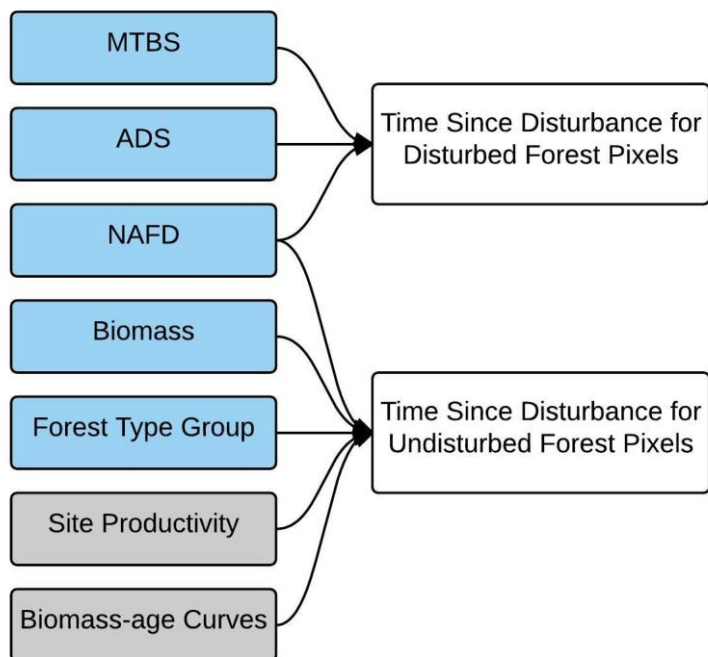
2   **Fig. 1.** Data sources for inferring time since disturbance for disturbed and undisturbed forest pixels. Blue boxes indicate data
3   derived from remote sensing data, and gray boxes are data compiled from FIA field data.
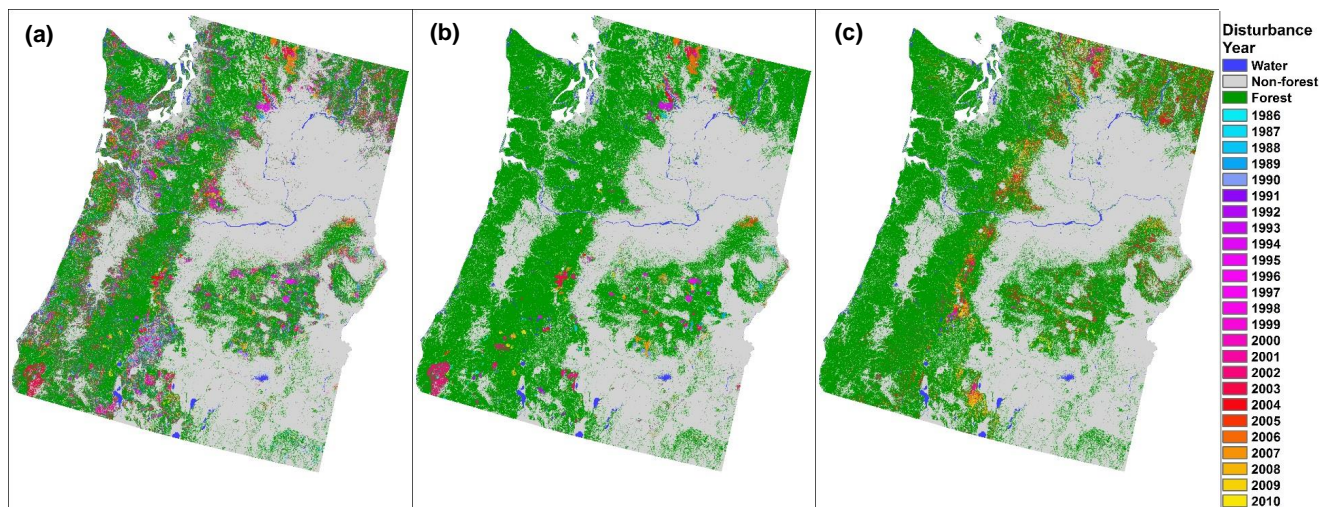
Fig. 2. Year of last disturbance from (a) NAFD, (b) MTBS and (c) ADS data of the PNW region. The time period for NAFD, MTBS and ADS datasets are 1986-2010, 1986-2010 and 1997-2010 respectively.
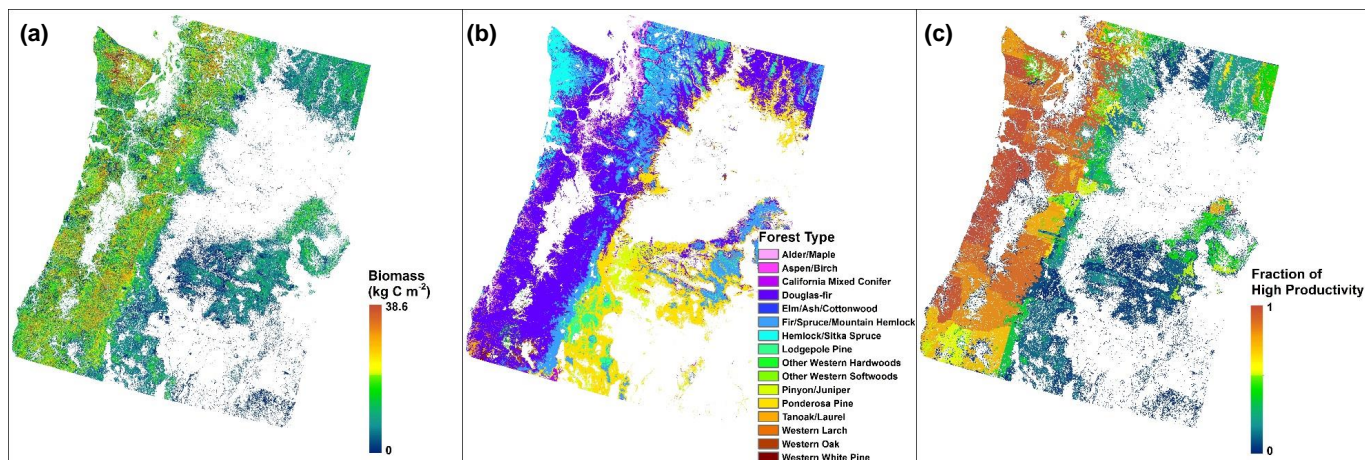
2 **Fig. 3.** Maps of (a) aboveground biomass, (b) forest type group and (c) site productivity in the PNW region.
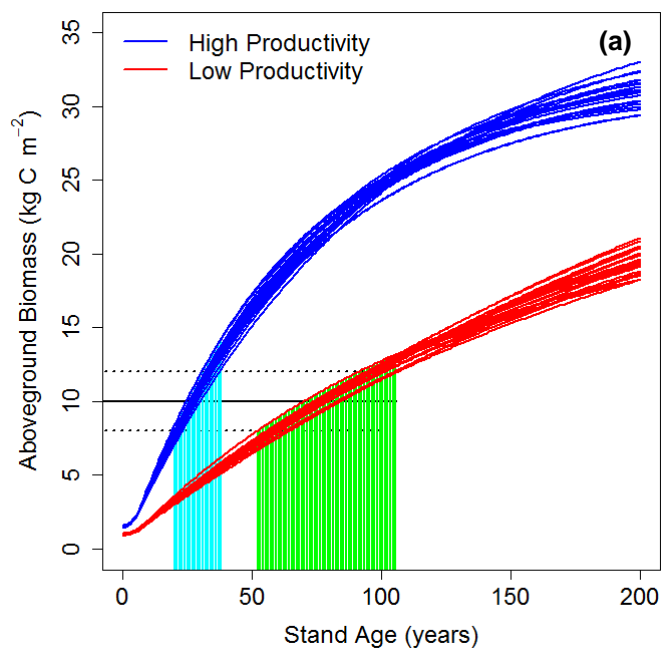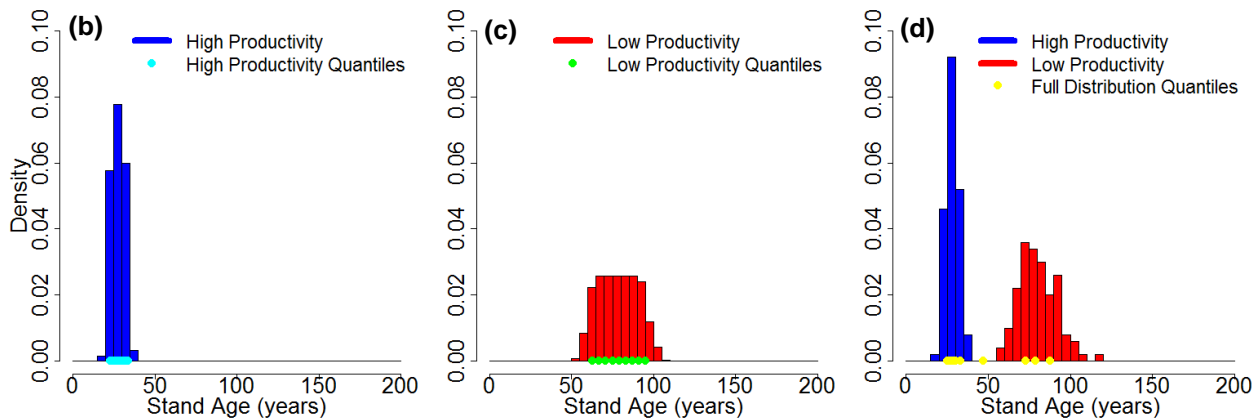
Fig. 4. Stand age inferred based on field inventory-derived species-specific biomass-age curves (a) for a forest pixel of the same forest type group with aboveground biomass of 10 kg C m^{-2} and having no recent disturbance. Histogram and quantiles of stand ages are shown for three site productivity classes: (b) high productivity site ($f_{high} = 1$), (c) low productivity site ($f_{high} = 0$), and (d) mixture of high and low productivity sites ($f_{high} = 0.6$).
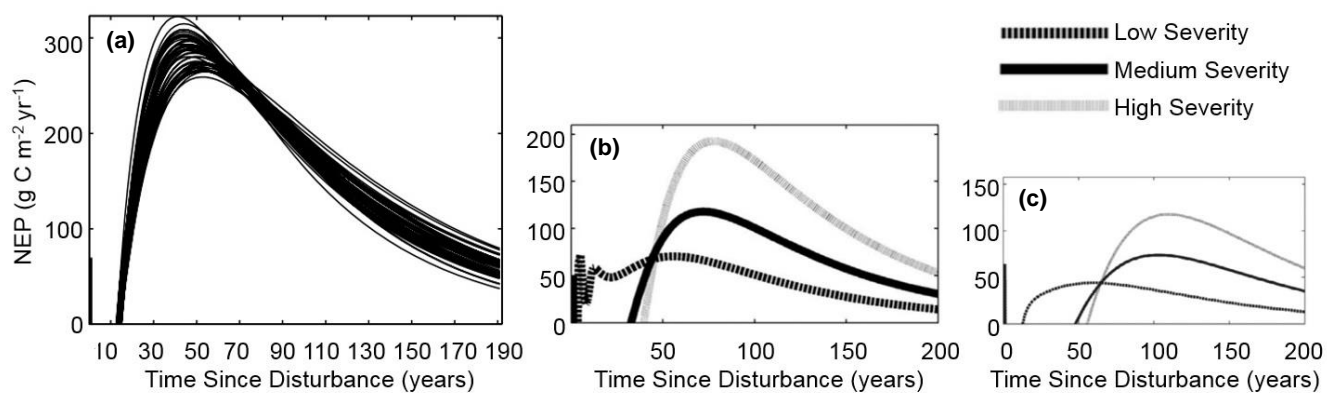
2 **Fig. 5.** Carbon flux trajectories of (a) post-harvest (Williams et al., 2012), (b) post-fire (Ghimire et al., 2012), and (c) post-beetles (Ghimire et al.,
3 2015) for a range of severities in high site productivity Douglas-fir stands of the PNW region.
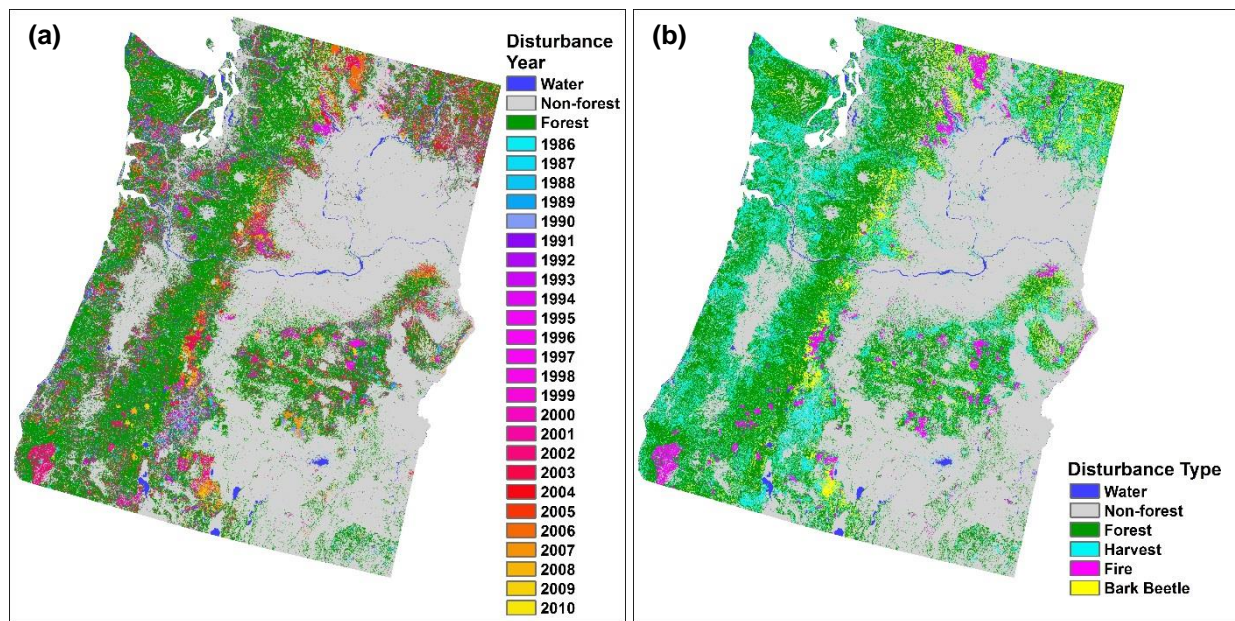
2   **Fig. 6.** Maps of (a) disturbance year and (b) disturbance type derived from NAFD (Fig. 2a), MTBS (Fig. 2b) and ADS (Fig.

3   2c) data in the PNW region.
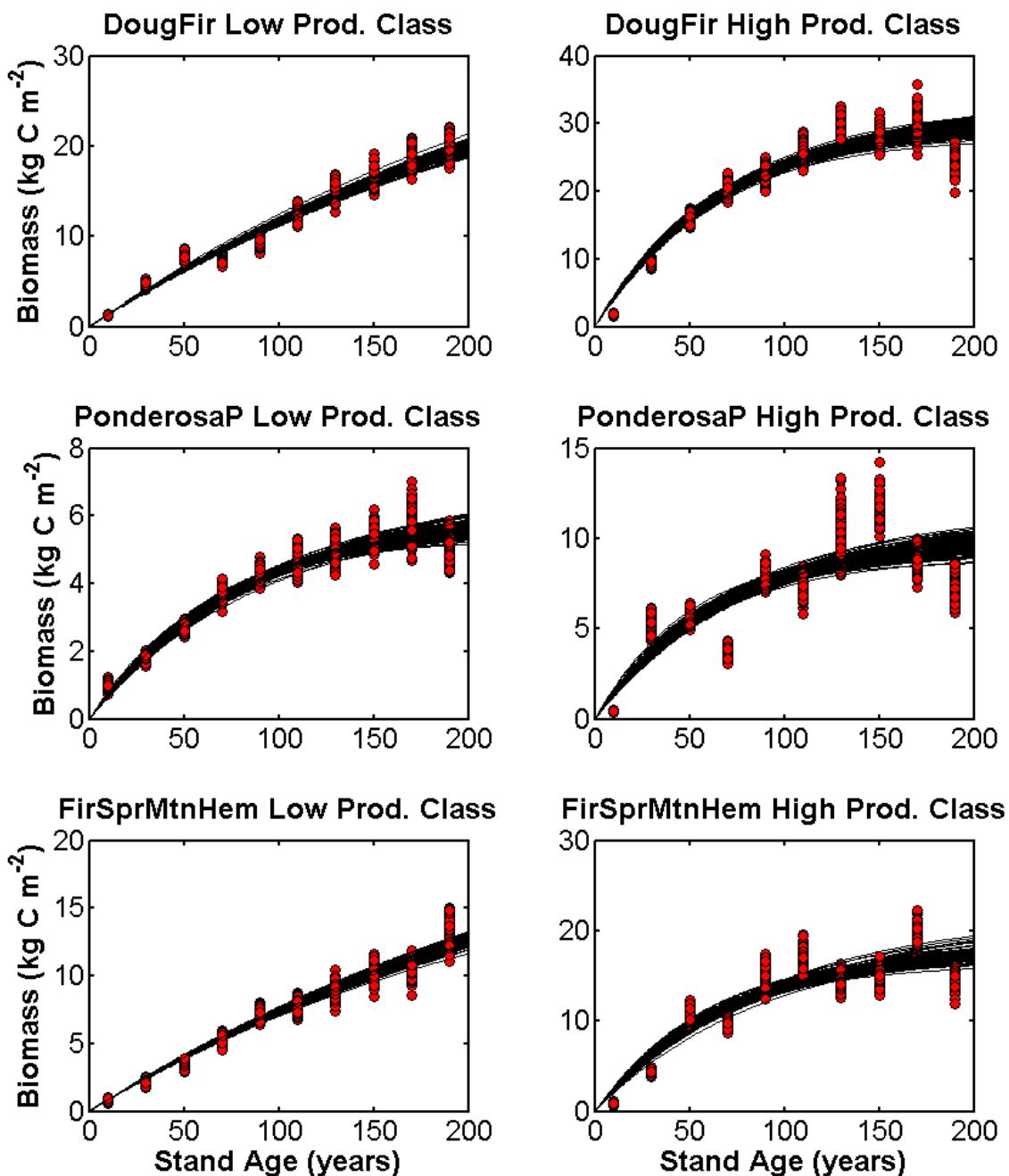
Fig. 7. Biomass-age curves sampled from FIA data for each forest type group and site productivity class in the PNW region. Curves for the three most abundant forest type groups are shown (DougFir is Douglas-fir, Ponderosa P is ponderosa pine, and FirSprMtnHem is fir/spruce/mountain hemlock). Red dots are independent samples drawn probabilistically from the FIA data.
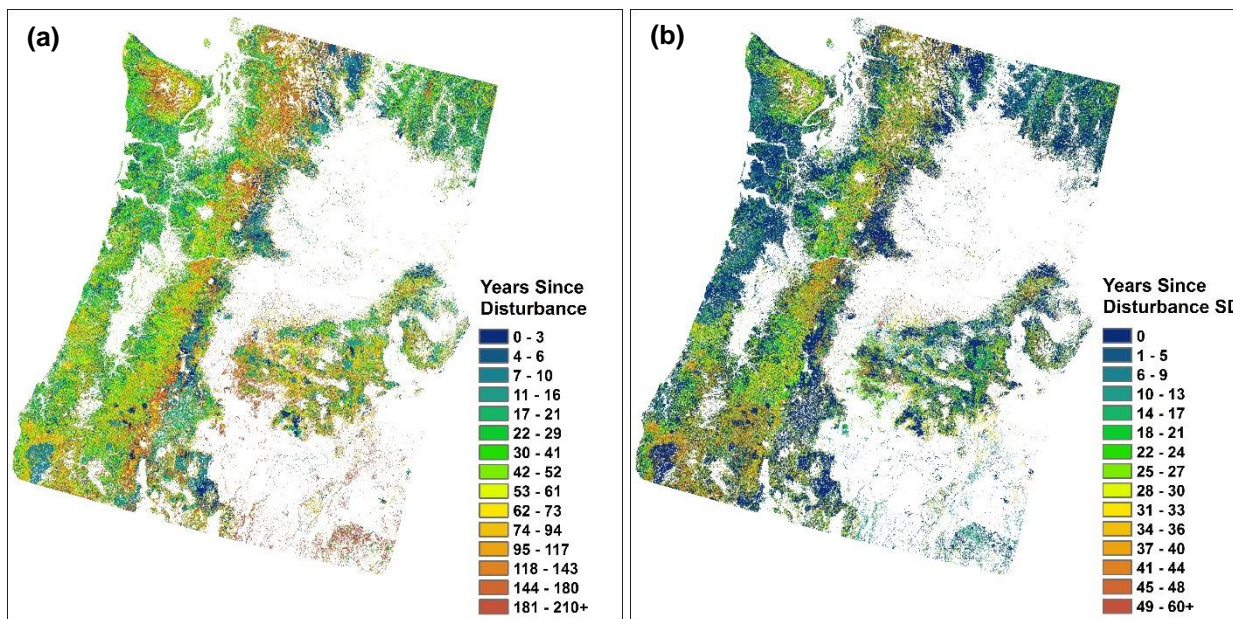
Fig. 8. Maps of (a) years since disturbance and (b) standard deviation in 2010 in the PNW region.
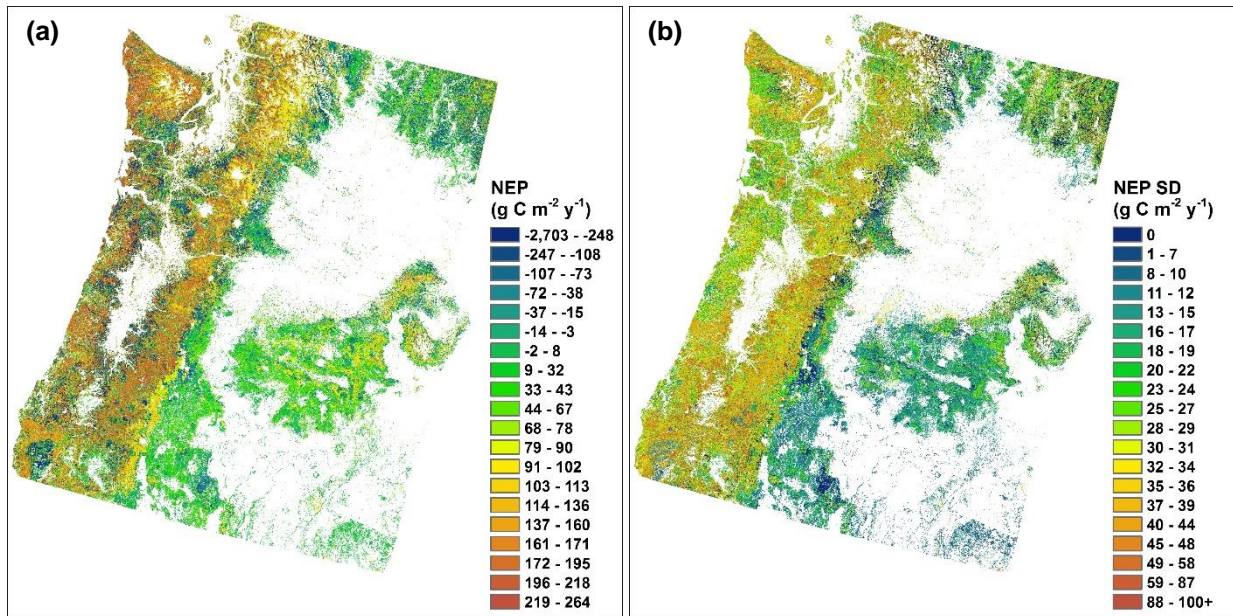
Fig. 9. Maps of (a) net ecosystem productivity (*NEP*) and (b) standard deviation in 2010 in the PNW region.
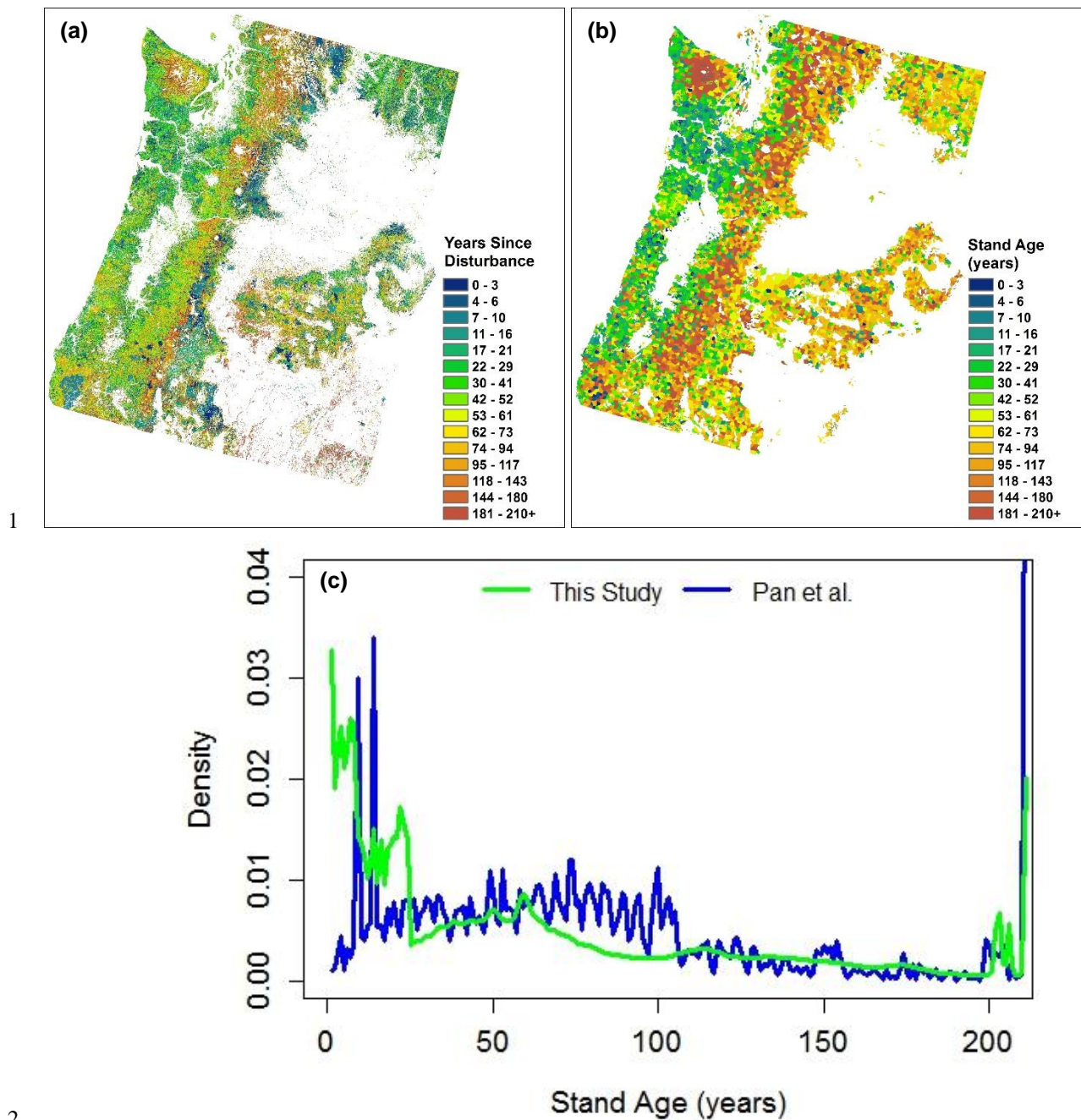
3 **Fig. 10.** Maps of stand age from (a) this study (same as Fig. 8a) and from (b) Pan et al. (2011) in the PNW region, associated
4 density curves of stand age were plotted in (c).
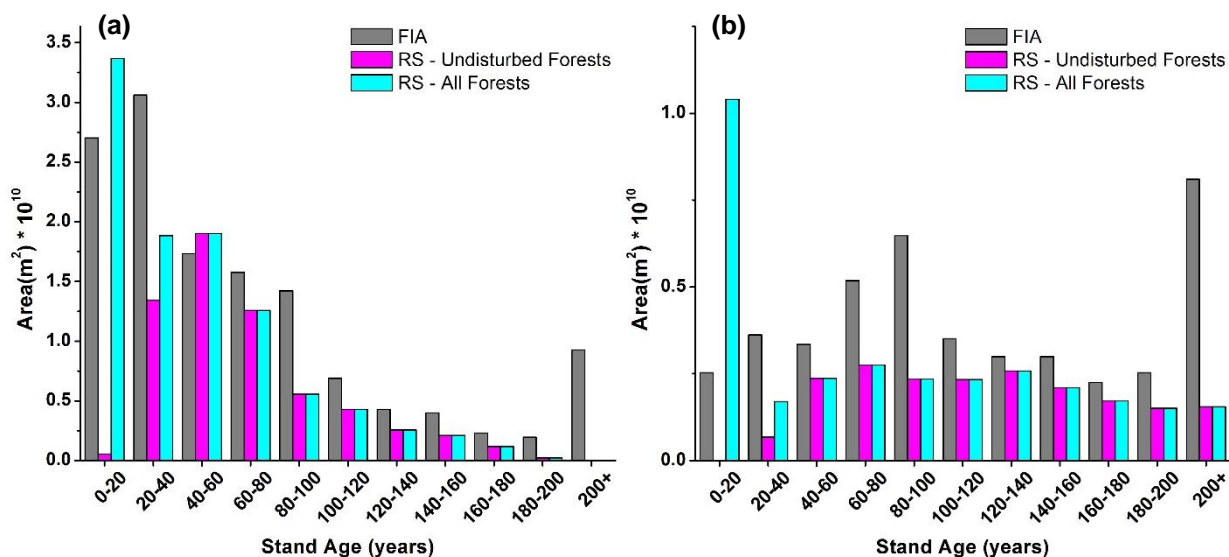
2   **Fig. 11.** Distribution of forest area by age for (a) Douglas-fir and (b) Fir-Spruce-Mountain Hemlock of the PNW region
3   comparing results from FIA data and remote sensing derived (RS-) estimates for undisturbed and all forests including those
4   marked as disturbed in NAFD, ADS, and MTBS datasets and shown here as if they were stand clearing events.